Atmos. Chem. Phys. Discuss., 10, 24919–24960, 2010
www.atmos-chem-phys-discuss.net/10/24919/2010/
doi:10.5194/acpd-10-24919-2010

Atmospheric Chemistry and Physics Discussions

Impacts of water vapor/aerosol loading trends and land cover on aerosol microphysical and radiative effects on clouds during the Amazon biomass burning season

J. E. Ten Hoeve[1], **L. A. Remer**[2], **and M. Z. Jacobson**[1]

[1]Department of Civil and Environmental Engineering, Stanford University, CA, USA
[2]NASA Goddard Space Flight Center, Greenbelt, MD, USA

Received: 11 August 2010 – Accepted: 27 September 2010 – Published: 25 October 2010

Correspondence to: J. E. Ten Hoeve (tenhoeve@stanford.edu)

Published by Copernicus Publications on behalf of the European Geosciences Union.

Abstract

High resolution aerosol, cloud, water vapor, and temperature profile data from the Moderate Resolution Imaging Spectroradiometer (MODIS) are utilized to examine the impact of aerosols on clouds during the Amazonian biomass burning season in Rondônia, Brazil. It is found that increasing background column water vapor (CWV) throughout this transition season between the Amazon dry and wet seasons likely exerts a strong effect on cloud properties. As a result, proper analysis of aerosol-cloud relationships requires that data be stratified by CWV to account better for the influence of background meteorological trends. Previous studies of aerosol-cloud interactions over Amazonia have ignored the systematic changes to meteorological factors during the transition season, leading to possible misinterpretation of their results. Cloud fraction is shown to increase or remain constant with aerosol optical depth (AOD), depending on the value of CWV, whereas the relationship between cloud optical depth (COD) and AOD exhibits a different relationship. COD increases with AOD until AOD~0.25, which is assumed to be due to the first indirect (microphysical) effect. At higher values of AOD, COD is found to decrease with increasing AOD, which may be due to: (1) the inhibition of cloud development by absorbing aerosols (radiative effect/semi-direct effect) and/or (2) a possible retrieval artifact in which the measured reflectance in the visible is less than expected from a cloud top either from the darkening of clouds through the addition of carbonaceous biomass burning aerosols within or above clouds or subpixel dark surface contamination in the measured cloud reflectance. If (1) is a contributing mechanism, as we suspect, then a linear relationship between the indirect effect and increasing AOD, assumed in a majority of global climate models, is inaccurate since these models do not include treatment of aerosol absorption in and around clouds. The relationship between aerosols and both CWV and clouds over varying land surface types is also analyzed. The study finds that the difference in CWV between forested and deforested land is not correlated with aerosol loading, supporting the assumption that temporal variation of CWV is primarily a function of the larger-scale meteorology.

ACPD
10, 24919–24960, 2010

However, a difference in the response of cloud fraction to increasing AOD is observed between forested and deforested land. This suggests that dissimilarities between other meteorological factors, such as atmospheric stability, may have an impact on aerosol-cloud correlations between different land cover types.

1 Introduction

The effect of aerosol particles on the hydrological cycle remains one of the largest uncertainties in our climate system. Biomass burning, from both deforestation and annual agricultural burning, is the largest anthropogenic source of such particles in the Southern Hemisphere. A variety of observational and modeling studies have examined the effect of aerosols on the regional hydrometeorology over the Amazon Basin during the biomass burning season (Kaufman and Nakajima, 1993; Kaufman and Fraser, 1997; Koren et al., 2004, 2008; Feingold et al., 2005; Yu et al., 2007; Zhang et al., 2008; Martins et al., 2009). Biomass burning aerosols have been shown to affect clouds through both microphysical and radiative mechanisms (Kaufman et al., 2005a; Kaufman and Koren, 2006; Koren et al., 2008; Rosenfeld et al., 2008). Depending on the concentration of aerosol, its chemical composition, size distribution, vertical distribution relative to clouds, and the background cloud characteristics, biomass burning aerosols are suggested either to inhibit or invigorate cloud formation and/or growth (Feingold et al., 2005; Koren et al., 2008).

Carbonaceous biomass burning aerosols can absorb solar radiation, warming the aerosol layer and reducing the radiation reaching the surface (Ackerman et al., 2000; Kaufman et al., 2002; Koren et al., 2004). This effect cools the surface, increases the static stability of the lower troposphere, suppresses surface heat and moisture fluxes, and slows the hydrological cycle (Jacobson, 2002; Andreae et al., 2004; Ramanathan et al., 2005). Evaporation of clouds within the aerosol layer may also occur due to the increase in temperature and decrease in relative humidity caused by aerosol absorption of solar radiation (Yu et al., 2002; Jacobson, 2006). Referred to as absorptive

ACPD
10, 24919–24960, 2010

effects or the semi-direct effect, these radiative processes primarily suppress the formation and growth of clouds.

Microphysical effects, on the other hand, enhance cloud formation and growth. Biomass burning aerosols are hygroscopic and can serve as cloud condensation nuclei (Feingold et al., 2001; Andreae et al., 2002, 2004). Expansion chamber experiments have shown that the addition of cloud condensation nuclei will nucleate a larger number of smaller cloud droplets, and these droplets are therefore slower to coalesce to form precipitation (Gunn and Phillips, 1957; Squires et al., 1958). These aerosol-processed clouds are also more reflective, exhibit changed drizzle properties, and have been suggested to have longer lifetimes (Twomey, 1977; Albrecht, 1989). However, the apparent darkening of clouds by absorptive biomass burning aerosols has also been observed by satellite (Kaufman and Nakajima, 1993; Wilcox et al., 2009). Recent studies have shown that these polluted clouds may become invigorated with higher liquid or ice water paths and lower cloud top pressures (Andreae et al., 2004; Khain et al., 2005; Koren et al., 2005, 2008; Lin et al., 2006; Rosenfeld et al., 2008; Meskhidze et al., 2009). The delay of raindrop formation in polluted clouds suppresses downdrafts, which allows for the generation of greater updrafts and stronger convection. The updrafts carry water vapor to higher altitudes, where additional energy from the latent heat of freezing may be released, further invigorating convection (Williams et al., 2002; Andreae et al., 2004; Rosenfeld et al., 2008). Increases in aerosol optical depth (AOD) have also been linked to increases in cloud fraction, particularly at low AODs (Kaufman et al., 2005a; Koren et al., 2005; Lin et al., 2006; Myhre et al., 2007).

More recent studies have illustrated that there may be a smooth transition between these competing microphysical and radiative effects (Koren et al., 2008; Rosenfeld et al., 2008). Using MODIS data over the Amazon, Koren et al. (2008) hypothesized that microphysical processes dominate at lower AODs, increasing cloud fraction and height, whereas radiative processes dominate at higher AODs, decreasing cloud fraction and height. The study also showed that the relative contributions of the microphysical and radiative effects are strongly tied to the *initial* cloud fraction prior to the influence

ACPD
10, 24919–24960, 2010

of aerosols – the radiative absorption effect begins to dominate at lower values of AOD for lower initial cloud fractions. This is due to the hypothesized aerosol absorption cloud fraction feedback: Stabilization of the near-surface atmosphere due to aerosol absorption of radiation initially reduces cloudiness, which then exposes more of the aerosol layer, further reducing cloudiness (Koren et al., 2008). Eventually, the reduction in cloudiness will allow sufficient surface heating to destabilize the lower atmosphere and reverse the positive feedback. This reduction in cloudiness has also been described as a black carbon-low cloud positive feedback loop (Jacobson, 2002). For low cloud fractions, more of the aerosol layer is available for absorption, resulting in a stronger feedback. For higher cloud fractions, microphysical invigoration will dominate for the same degree of aerosol loading. An implication of this finding is that aerosol effects on either sparse or dense cloud fields may have entirely opposite effects on climate forcing.

For the majority of observational biomass burning studies over the Amazon, the months of August, September, and October are typically selected due to the combination of high aerosol loading from biomass burning and consistent dry conditions present during these months. The Amazon dry season occurs during the Southern Hemisphere winter, and is defined by a subtropical high pressure that resides over the Amazon Basin (Nobre et al., 1998). Felled vegetation is allowed to dry out during the season, and is burned during the Southern Hemisphere spring. High pressure typically remains over the region until mid-to-late October, when the onset of the rainy season begins (Nobre et al., 1998). Small cumulus clouds often form at the top of the atmospheric boundary layer, which is constrained by a subsidence inversion. Biomass burning smoke is generally mixed within the boundary layer (Davidi et al., 2009). Occasionally, smoke plumes are pumped out of the boundary layer through deeper cumulus convection; however, the majority of biomass burning smoke exists at or below the cloud layer at an approximate altitude of 3 km (Davidi et al., 2009). Higher cold clouds, decoupled from the smoke below, also occur at times.

ACPD
10, 24919–24960, 2010

During the biomass burning season, cloud properties are assumed to be weakly dependent on meteorology due to the stationary high pressure overhead (Kaufman and Nakajima, 1993; Koren et al., 2004, 2008). However, our study illustrates that gradually increasing background column water vapor (CWV) during the biomass burning transition season between the end of the dry season and the beginning of the wet season, has a discernable impact on aerosol-cloud relationships. Previous studies have noted that aerosol loading and CWV are weakly spatially correlated over the Amazon Basin on seasonal timescales (Feingold et al., 2001). On smaller spatial and temporal scales, latitudinal variation of both CWV and AOD will produce high correlations in some areas (Kaufman and Fraser, 1997). Regions where simultaneous advection of these two parameters takes place also exhibit high correlations (Remer et al., 1998). However, these studies do not take into consideration inconsistent sampling resulting from temporal correlations between CWV and AOD on longer timescales. Variability in CWV, which can be observed daily at relatively high spatial resolution using the MODIS sensor, may be used as a tracer for large-scale meteorological variability. Attempts to remove the influence of meteorology from aerosol-cloud correlations are common (Koren et al., 2005; Lin et al., 2006; Yu et al., 2007). Here, we use CWV, which is also shown to correlate well with MODIS cloud parameters, to stratify the aerosol and cloud data.

The latter portion of the paper tests the assumption that CWV is not influenced by aerosol loading, which is assumed in the former portion of the paper, by analyzing effects of aerosols on CWV and clouds over different land surface types. Many studies have probed the local effects of deforestation on local and regional meteorology; however, no observational studies have analyzed the aerosol effect on clouds over both forested and deforested land. Studies have examined the regional climate effects of deforestation through changes in surface energy and water vapor fluxes and land-atmosphere interactions (Henderson-Sellers and Gornitz, 1984; Nobre et al., 1991; Cutrim et al., 1995; Wang et al., 2000; Roy et al., 2002; Negri et al., 2004; Wang et al., 2009). Depending on the structure and scale of the deforestation, contrasting effects

ACPD
10, 24919–24960, 2010

on clouds and precipitation are observed (D'Almeida et al., 2007). Smaller scale deforestation (i.e. the fish bone pattern) spawns mesoscale circulations that arise from land surface heterogeneities on the finer scale (Segal et al., 1988; Wang et al., 2000, 2009; Roy et al., 2002). Enhanced shallow convection over deforested regions is caused in part by a land breeze from nearby moisture-rich forests. When this moist land breeze reaches unstable air over the deforested region (due to greater surface heating), it rises to form clouds (Segal et al., 1988; Roy et al., 2002). Several observational studies have shown an increase in shallow convection over disturbed regions of the Amazon due to this direct thermal circulation, particularly in the state of Rondônia, Brazil (Cutrim et al., 1995; Durieux et al., 2003; Negri et al., 2004; Wang et al., 2009). Our study differs from previous studies in that the aerosol effect on water vapor and clouds over forested and deforested land is examined – a logical extension of the studies noted above.

The timescale of cumulus clouds in our region of interest is on the order of minutes, yet these clouds are organized into cloud fields that have a much longer duration, influenced by surface properties as well as local mesoscale and larger circulations. Cloud fields generally form by noon and dissipate overnight throughout the Amazon Basin (Koren et al., 2004). Cloud fields resulting from the land breeze between forest and pasture also vary on diurnal time scales. Aerosol loading, conversely, may vary on longer weekly time scales even if source fires vary diurnally (Giglio, 2007). Biomass burning smoke can build over many diurnal cycles and thus become more homogenous both temporally and spatially than the individual clouds or cloud fields.

Accounting for meteorological variability in observational aerosol-cloud correlation studies is paramount. The aerosol effect on cloud properties over the Amazon has been shown to differ in a humid year compared to a dry year (Yu et al., 2007). Our study incorporates both dry and wet years, reducing this interannual variability, while also stratifying the data by CWV to ensure similar background moisture conditions exist along the range of AOD retrievals used. This study investigates two primary questions: (1) how can contamination from meteorological variability in observed aerosol-cloud relationships be reduced and (2) what is the aerosol effect on column water vapor and

ACPD
10, 24919–24960, 2010

clouds over different land surface types.

2 Data and methods

MODIS, onboard the Terra and Aqua satellites, provides relatively high spatial resolution (250–500 m) while achieving near global coverage on a daily basis (Salomonson et al., 1989). The daytime Aqua overpass (01:30 p.m. LT) is chosen over the Terra overpass (10:30 a.m. LT) since clouds are more likely to be developed in the afternoon than the morning. MODIS is chosen over other sensors, such as the Multi-angle Imaging Spectroradiometer (MISR), due to its high resolution and because MODIS produces a variety of cloud and atmospheric profile products, which other sensors do not (Diner et al., 1998). This study employs MODIS Swath Level 2 aerosol, cloud, water vapor, and temperature products (King et al., 2003). Data from these products, which are provided at resolutions between 1-km and 5-km, are upscaled to match the aerosol product resolution at 10-km. We create an aggregated product with multiple satellite parameters at a scale which is considerably finer than the $1^{\circ}\times1^{\circ}$ Level 3 product.

Aerosol optical depth from the aerosol product is calculated over land and ocean at a wavelength of 550 nm, with a footprint of 10-km×10-km (Kaufman et al., 1997; Remer et al., 2005; Levy et al., 2007). Surface reflectances utilized in the aerosol algorithm are dynamic, and related to empirical functions which match reflectances in the near-infrared wavelengths to visible wavelengths in order to calculate an NDVI-like measure of vegetation and geometry (Levy et al., 2007). Validation with ground-based AERONET observations yield an overall error of $\pm0.05\pm0.15\,\tau_a$ over land, where τ_a is the aerosol optical depth at 550 nm (Levy et al., 2007).

The Level 2 cloud product produces retrievals of cloud fraction, cloud top properties, cloud phase properties, and cloud microphysical properties, calculated using up to fourteen of the thirty-six MODIS spectral bands (Ackerman et al., 1998). The cloud fraction and cloud top properties are produced at 5-km×5-km resolution, whereas the microphysical properties are produced at 1-km×1-km resolution (Platnick et al., 2003).

ACPD
10, 24919–24960, 2010

The 5-km cloud fraction product is computed using the fraction of 1-km cloudy pixels in the 5-km footprint, as determined by the cloud mask product (Platnick et al., 2003).

The cloud microphysical properties include cloud optical depth (thickness), cloud effective radius, and cloud water path. Cloud optical depth is inversely calculated from spectral reflectance measurements and surface albedo data by using a lookup table (Nakajima and King, 1990; Platnick et al., 2003). For over-land retrievals, cloud optical depth is calculated at wavelengths 0.645 µm and 2.130 µm. The 1-km and 5-km cloud data are averaged into 10-km×10-km grid boxes in order to conform to the Level 2 aerosol data. A drawback of the MODIS sensor is that it cannot discern the vertical location of aerosols or the physical thickness of clouds. As a result, additional sensors (e.g. the CALIPSO lidar) are required to study the vertical distribution of clouds and aerosols (Winker et al., 2003).

Column water vapor (precipitable water vapor) is derived by integrating the 101 levels at which water vapor mixing ratios are calculated in the MOD07 atmospheric profile product (Seemann et al., 2003). Units are reported in centimeters of equivalent liquid water. We choose not to use the near-IR column water vapor product due to its limitations over dark surfaces (Gao and Kaufman, 2003). Temperature profile observations are also employed from the MOD07 product to estimate low-level stability (Seemann et al., 2003). Since surface pressure is often below 1000 hPa, the temperature at 1000 hPa is calculated using the skin temperature, surface pressure, and Poisson's equation for potential temperature. Skin temperature is not the best approximation for surface air temperature; however, for the purposes of finding relative differences in atmospheric stability across our study domain, we feel this is our best option considering that a high-resolution observational surface temperature data set is currently not available from any other source. The water vapor and temperature products are produced at 5-km resolution, and are averaged to the 10-km scale to conform to the Level 2 aerosol data. Products requiring a clear sky, such as the atmospheric profile products, are able to be estimated for a significant number of 10-km pixels with cloud fractions less than one.

ACPD
10, 24919–24960, 2010

In the first portion of the paper, aerosol and cloud data over all non-water surfaces are included in the analyses. In the latter portion of the paper, MODIS aerosol, cloud, stability, and water vapor data are stratified by land cover type. This requires an up-to-date, high-resolution land cover classification data set. The Land Processes Distributed Active Archive Center (LP DAAC), located at the U.S. Geological Survey (USGS) Earth Resources Observation and Science (EROS) Center, provides a combined Terra/Aqua yearly land cover product – MCD12Q1 (http://lpdaac.usgs.gov). This product employs decision tree classification algorithms and training data to assign land cover classifications (Friedl et al., 2010). The data are resampled from 500-m×500-m resolution to 0.1°×0.1° resolution to approximately match the resolution of the Level 2 swath aerosol data.

Our 5°×5° study region encompasses the deforested region of Ji Paraná in Rondônia, Brazil, as well as a protected forest to the east, illustrated in Fig. 1. Broadleaf forest classifications are assigned to the forested category, whereas closed shrublands, open shrublands, woody savannas, savannas, grasslands, croplands, cropland and natural vegetation mosaic, and barren or sparsely vegetated classifications are assigned to the deforested (pasture) category, according to the International Geosphere-Biosphere Programme categorization scheme (Friedl et al., 2010). The percentage of deforested land increases with time in our fixed study region due to ongoing forest conversion activities.

A small region is chosen for this study, compared with other studies of its type, so that meteorological differences due to spatial variation will be better removed, and so that stratification of atmospheric data by land cover type can be conducted. The high spatial resolution of the Level 2 data allows for the accumulation of a sufficient data record for analysis, while also reducing the pixel size in which aerosol and cloud characteristics need to be assumed constant, compared to Level 3 data which is produced at a resolution of 1°×1°. The study encompasses the Amazonian biomass burning months of August, September and October for the years 2004 through 2007. This time period includes both dry and wet years, as well as years with both heavy and light biomass

ACPD
10, 24919–24960, 2010

burning, according to NCEP/NCAR Reanalysis data and MODIS data (Kalnay et al., 1996; Koren et al., 2007). The inclusion of multiple years reduces the interannual variability present in the data, and also allows for the compilation of a large enough data set for analysis in our small study region.

Retrievals that are not considered "useful" or were considered "bad" quality according to the Level 2 quality assurance bit data were removed. To account further for meteorological variability, NCEP/NCAR Reanalysis 700 hPa wind vectors are used to remove days for which the South Atlantic subtropical high was not the dominant weather pattern over the region (Kalnay et al., 1996). Scattered small cumulus clouds which develop each afternoon are most prevalent during this season, yet deeper convective clouds are occasionally observed (Koren et al., 2004). By removing these anomalous days, cloud fields are more likely to be similar among all days analyzed, even though the structure and morphology of these clouds are already similar throughout this season. We removed a total of 43 days during our study period, equaling 12% of the total number of days in August through October between 2004 and 2007. We restrict the number of cloud types analyzed by choosing to study only warm clouds. Warm clouds are segregated from cold and unknown-phase clouds by only retaining 10-km pixels that contain >95% of 1-km cloud retrievals in the liquid water phase. We have retained a total of 368 288 warm cloud and clear sky retrievals over our domain and study period. The re-sampled 10-km atmospheric aerosol, cloud, and profile data are then segregated by forested and deforested land cover types in the latter portion of the paper to explore the effect of land-atmosphere-aerosol interactions on column water vapor and clouds.

Aerosol optical depth and column water vapor MODIS satellite retrievals are compared with Aerosol Robotic Network (AERONET) automatic sun/sky radiometer data in Fig. 2 (Holben et al., 1998). Data represent two stations within the 5°×5° study region, Abracos Hill, active in 2004 and 2005, and Ji Paraná SE, active in 2006 and 2007. Only days that fall within our study period are included. Correlation coefficients between MODIS and AERONET retrievals are above 0.90 for both aerosol optical depth

ACPD
10, 24919–24960, 2010

and column water vapor, providing confidence in the MODIS satellite retrievals.

3 Results

3.1 Effect of water vapor and aerosol loading trends

Column water vapor (CWV) increases over our study region throughout the dry-to-wet transition season between the months of August to October. Figure 3a shows MODIS CWV and warm cloud fraction averaged into eight equally-spaced bins between 1 August and 31 October, for all years between 2004 and 2007. Cloud fraction and CWV are understandably highly positively correlated, as water vapor is one of the principal components required for cloud formation. Figure 3b shows MODIS aerosol optical depth (AOD) at 550 nm, also binned by day of the season. Unlike CWV, AOD increases from 1 August until approximately the middle of September, at which point the trend reverses and decreases until the end of the season on 31 October. This mid-season peak in aerosol loading is indicative of a biomass burning peak that is largely determined by social behavior (Crutzen and Andreae, 1990). Burning usually occurs late enough into the season to sufficiently allow vegetation to dry out, but not too late to risk an early onset of the rainy season.

Figure 3c and d depict the same time series as Fig. 3a and b, but for AODs less than or equal to 0.8. AODs are restricted to below 0.8 for the remainder of the analysis to prevent aerosol misclassification as cloud (Brennan et al., 2005). In this range, significant cloud contamination of aerosol is also unlikely, yet occasional contamination may still occur (Kaufman et al., 2005b). Koren et al. (2010) found that MODIS aerosol-cloud correlations over the tropical Atlantic were likely affiliated with physical mechanisms and not retrieval artifacts, suggesting a similar relationship for our study region. It is also improbable that these correlations are due to a 3-D cloud effect, which artificially increases AOD retrievals in the regions neighboring clouds (Wen et al., 2006). This effect has been suggested to be larger for greater cloud cover and aerosol loading, but

ACPD
10, 24919–24960, 2010

our results indicate that the strongest positive correlation between cloud fraction and AOD occurs at lower values of AOD and cloud cover (see discussion of Fig. 4 below) (Wen et al., 2006; Yu et al., 2007). Time series trends of cloud cover and water vapor loading are similar between Fig. 3a and c. Trends of aerosol loading between Fig. 3b and d are also similar, suggesting an analogous behavior for low AODs compared to the case which contains all data.

Figure 3 indicates that CWV and cloud fraction are directly correlated with AOD during the first half of the season, whereas these variables are inversely correlated during the second half of the season. Thus, if we plot CWV and cloud fraction directly against AOD, separated into the two halves of the season, we would expect the signs of the regression slopes to be the same for each parameter in each half season. If CWV increases with aerosol in the first half season, then so should cloud fraction. If CWV and AOD are negatively correlated in the second half season, then cloud fraction should also be negatively correlated with AOD.

Figure 4a shows CWV binned by AOD for all non-zero cloud fraction retrievals in our study region for the same time period as in Fig. 3. The data are stratified by day of the season, with plots representing each half of the season and all days in the season. Figure 4b depicts warm cloud fraction binned by AOD, for the same periods as in Fig. 4a. In these figures, cloud properties and CWV are binned by AOD, with each bin representing 12.5 percentile of the AOD values. This method has been used previously in other studies so that bias is not introduced through inconsistent sampling in each bin (Lin et al., 2006). The absolute low and high AOD boundaries are assigned to be 0.05 and 0.8, however, the location of individual bin edges vary for each plot. The bin centers are defined as the average AOD value in each bin and error bars representing the standard errors of the bin average ($\sigma/N^{1/2}$) are also included.

In the first half season, 1 August to 15 September, there is a positive correlation between both CWV and AOD, as well as between cloud fraction and AOD, as expected from Fig. 3. However, in the second half season, 15 September to 31 October, CWV is negatively correlated with AOD as expected, but cloud fraction is not. This deviation

ACPD
10, 24919–24960, 2010

of the cloud fraction relationship to AOD in a direct correlation overrides the controlling effect of the seasonal CWV evolution on cloud formation and strongly points to aerosol as a modifying element of cloud properties. We conclude that both large-scale meteorological factors traced by seasonally-varying CWV and aerosol loading may contribute to changes in warm cloud fraction in our region of interest.

This conclusion has important implications for analyzing aerosol-cloud interactions. Following previous studies, common practice would be to accumulate all pixels with both aerosol and cloud retrievals during the biomass burning season, and then bin the cloud retrievals by AOD, implicitly assuming constant meteorological conditions throughout this period (Koren et al., 2004, 2008). However, this study finds that embedded in these correlations are systematic variations in CWV with AOD. As a result, this CWV signal may impact aerosol-cloud correlations. For example, the "boomerang" shape identified by Koren et al. (2008) and attributed to the combination of microphysical and radiative effects by aerosols on clouds may also contain an element of within-season evolution of the meteorological conditions and source variations. In Fig. 4a we identify a boomerang shape in the CWV vs. AOD plot that is due solely to the combination of the different halves of the season, and not a physical consequence of the aerosol at all. The similar boomerang shape in cloud fraction over the full biomass season seen in Fig. 4b reflects both the actual relationship between cloud fraction and aerosol in the latter half season and also the artifact created by combining the two half seasons.

Figure 4c and d shows CWV and cloud fraction again binned by AOD, but only for cloud fractions less than 0.5. By retaining only low cloud fractions, more of the aerosol layer is exposed to sunlight in each 10-km×10-km retrieval box. In these scenes, it has been hypothesized that the increased aerosol exposure to sunlight will result in a stronger absorption effect on clouds and that the decrease of cloud fraction with AOD will begin at lower values of aerosol loading (Koren et al., 2008). The lower cloud fraction should not affect the relationship between CWV and AOD because CWV should not be affected by a warming atmospheric column. Indeed, Fig. 4c shows little

ACPD
10, 24919–24960, 2010

difference in both the shape of the graph and the magnitude of the change of CWV with AOD when compared with Fig. 4a.

Exposure to sunlight has little effect on CWV. However, consistent with Koren et al. (2008), we find that exposure to sunlight does affect the relationship between aerosol loading and cloud fraction. The less cloudy plot of Fig. 4d has shifted the turning point between increasing and decreasing cloud fraction to lower aerosol loading. Figure 4d locates the turning point at AOD=0.30–0.40, as opposed to the total data set of Fig. 4b where the turning point is at AOD=0.55. The boomerang relationships in Fig. 4a and d exist well outside the standard errors of the individual bins, a result which supports their statistical significance.

Figures 3 and 4 both confirm the associations between clouds and aerosols identified from satellite retrievals observed in previous studies and also sound a warning that some of these associations contain an artifact introduced from slowly evolving meteorological factors that can be traced by CWV. We note a difference between this study and the previous studies mentioned above. We are focusing on a very small ($5^{\circ} \times 5^{\circ}$) region in Rondônia, compared to previous studies, which took a broader view that included the entire Amazon Basin with its varied surface types, biomes and climatic zones. The trends shown in Fig. 3 are applicable for larger areas as well, but the range between low and high CWV and low and high AOD over the season becomes diluted as the study area is expanded. Our study area captures the strong seasonal variation in water vapor, cloud, and aerosol properties that still exists but in diluted magnitudes when our region is combined with surrounding areas.

We can identify the transition between meteorological seasons by using CWV as a tracer for the slow onset of the rainy season and stratify the data set using this parameter to control for meteorology. Figure 5a depicts CWV binned by AOD for all cloud fraction retrievals, and for five percentile groupings of CWV. Each grouping spans 16 percentile points, with a minimum percentile of 10% and a maximum percentile of 90% to avoid outlier values. These bounding low and high percentiles refer to CWV values of 2.10 cm and 5.33 cm, respectively. In general, lower percentiles represent

ACPD
10, 24919–24960, 2010

retrievals early in the season whereas higher percentiles represent retrievals late in the season. The number of retrievals per bin increases with CWV due to decreasing prevalence of cloud-free pixels between the beginning and end of the biomass burning season. In each grouping, CWV only varies marginally between AOD bins, with a maximum difference of 0.09 cm between any two bins in any grouping. This nominal variation in CWV within each grouping is likely to have only a minimal effect on cloud properties.

Figure 5b depicts cloud fraction binned by AOD for the five CWV groupings. The change in cloud fraction with AOD in Fig. 5b is more representative of the true aerosol effect on cloud fraction compared to Fig. 4 since the influence of varying CWV has been minimized. Cloud fraction increases with CWV, as indicated in Fig. 3a and c. For each CWV grouping, cloud fraction either exhibits a modest increasing trend, on average, across the AOD range between 0.05 and 0.8, or remains relatively constant along this range. The 42nd to 58th percentile grouping and the 58th to 74th percentile groupings do not exhibit an increasing trend to the extent of the other groupings. It is probable that increasing trends are absent in these middle CWV groupings due to the lack of low AODs during the mid-season peak of the biomass burning season. In this figure, the aerosol effect on cloud fraction does not appear to be largely dependent on CWV, which agrees with previous studies (Feingold et al., 2001).

The highest CWV grouping appears to demonstrate the greatest microphysical effect: cloud fraction increases at the greatest rate below an AOD of 0.35 compared to other groupings. In high water vapor loading environments, addition of aerosol at low AODs may increase cloud fraction to a greater extent than in lower water vapor loading environments, as also suggested in Yu et al. (2007). This result also agrees with the aerosol absorption cloud fraction feedback – the greater the initial cloud fraction, the greater the microphysical effect (Koren et al., 2008).

The flattening of these curves at higher AODs suggests a saturation of the microphysical effect. The absence of a strong aerosol absorption effect in Fig. 5b conflicts with some studies (Koren et al., 2004, 2008), but agrees with others depending on the

ACPD
10, 24919–24960, 2010

year analyzed (Lin et al., 2006; Yu et al., 2007). Part of the discrepancy may be due to the gradient of aerosol absorption properties north to south. The focus area of this study is embedded in the deforestation zone, with smoke having higher single scattering albedo (less absorption) than the smoke in the Cerrado to the south (Dubovik et al., 2002). A less absorbing smoke will have less radiative effect than the model formulated by Koren et al. (2008).

If the aerosol is affecting cloud microphysics, the signal should be apparent in the cloud optical depth (COD) as well in the cloud fraction. Figure 6a shows COD binned by AOD for the four highest CWV groupings in Fig. 5. According to the aerosol first indirect effect, increases in aerosol number loading increase the number concentration of cloud condensation nuclei, which in turn increase cloud reflectivity (Twomey, 1977). This effect would be observed as an increase in COD with increasing AOD in Fig. 6a. However, Fig. 6a illustrates that for all four CWV groupings, COD increases only to a certain AOD threshold between 0.2 and 0.3, and then decreases with increasing AOD. Note that Fig. 6a includes clouds at all stages of vertical development, as long as the clouds are in the liquid phase. While cloud fraction in Fig. 5 is highest for the highest CWV grouping and lowest for the lowest CWV grouping, COD behaves oppositely as clouds on average become thinner but cover a larger spatial area for higher CWVs later in the biomass burning season.

Figure 6b also shows COD binned by AOD, but only for pixels with average cloud top pressures between 800 hPa and 850 hPa. This range is roughly between the median and mean liquid water cloud top pressures over the 2004 to 2007 period. Figure 6b shows a similar boomerang pattern of COD versus AOD as Fig. 6a, except with more noise. Only a narrow range of cloud top pressures are retained to ensure that the COD versus AOD relationships observed in Fig. 6a are not merely the result of sampling clouds at different stages of growth. The AOD turning point of the boomerang in Fig. 6b occurs at generally higher AODs than in Fig. 6a, specifically for the lower two CWV groupings. In addition, the magnitude of the decrease in COD with increasing AOD in terms of percentage reduction from the peak is more similar among CWV groupings

ACPD
10, 24919–24960, 2010

than in Fig. 6a. This may be because in Fig. 6b, all clouds have similar cloud top pressures and are situated in more homogenous cloud fields.

The increase in COD with AOD for low aerosol loading may be explained by Twomey (1977) and follows from aerosol particles affecting the microphysics of the clouds. The decrease in COD with increasing AOD above AODs of 0.3 in Fig. 6a can be explained by a combination of physical processes and satellite retrieval artifacts. Physically, aerosol absorption of solar radiation can evaporate or thin clouds optically. However, satellite retrieval artifacts can also play a role. Carbonaceous aerosols within or above clouds (Kaufman and Nakajima, 1993), or subpixel holes in the clouds that reveal a dark surface beneath reduces the visible reflectance received by the satellite, and this is interpreted by the retrieval as a lower COD. In fact, a physical-artificial feedback can be started in which the aerosol begins to thin the cloud via radiative processes, revealing more holes that introduce darker visible reflectance to the satellite measurements. The microphysical effect dominates at lower AODs whereas the physical and artificial effects that decrease COD with aerosol loading are radiative in nature and will dominate at higher AODs. Considering that all of the aforementioned explanations for COD decrease are dependent on aerosol radiative absorption, the strength of the COD decrease should be inversely proportional to cloud fraction, because lower cloud fraction allows the aerosol greater exposure to sunlight. When the aerosol is exposed to sunlight, more aerosol translates to even higher rates of absorption and heating. The highest magnitude COD decrease occurs for the lowest CWV grouping with the lowest cloud fraction, and the lowest magnitude COD decrease occurs for the highest CWV grouping with the highest cloud fraction. This pattern is consistent with the hypothesis that the COD decrease is a radiative effect of the aerosols, whether the effect is physical or artificial or a combination of both.

Sorting out the exact cause of the COD decrease with increasing AOD is difficult. The absence of a strong absorption effect in the cloud fraction plots would suggest that darkening plays a role in the COD plots. Wilcox et al. (2009) found that biomass burning aerosols over a stratocumulus deck will artificially reduce cloud optical depths retrieved

ACPD
10, 24919–24960, 2010

by the MODIS sensor. The darkening bias was found to be greater for higher AODs, as expected, and also for higher non-polluted values of COD. Both of these relationships are observed in Fig. 6a. Unlike the Wilcox et al. (2009) study, the data in Fig. 6 do not consist only of scenarios with aerosols above clouds. Analysis of an individual day using both MODIS and the CALIPSO lidar, the latter of which has an overpass time roughly 1 min after the Aqua satellite and can detect the vertical distribution of clouds and aerosols, results in a similar boomerang trend in COD versus AOD even when the cloud layer forms at or above the top of the aerosol layer. Figure 7 shows the results of just one day, 12 August 2006, where clouds form above the aerosol layer and COD exhibits a boomerang trend with AOD. Figure 7a shows the CALIPSO vertical feature classification, with "bad" quality data masked, and Fig. 7b shows a scatter plot of COD and AOD retrievals from the MODIS Aqua sensor on this same day. A third degree polynomial function that best fits the data is also plotted, illustrating that COD increases with increasing AOD initially, but then decreases with increasing AOD at higher values of AOD similar to Fig. 6a.

Kaufman and Nakajima (1993) also hypothesized that biomass burning aerosol darkens Amazonian clouds due to the presence of black carbon inside clouds. This study found that cloud reflectance at 640 nm is reduced from 0.71 to 0.68 for an increase in aerosol optical depth between 0.1 and 2.0. This small decrease in visible reflectance is likely not the sole cause of decreases in COD between 20% and 50%, observed in Fig. 6a. Because of the modest role expected by the darkening of the clouds and the absence of a strong absorption effect in the cloud fraction plots, the physical-artificial feedback involving thinning clouds and increasing inclusion of dark reflectance from the surface beneath is the most promising explanation. Modeling studies have also found that black carbon absorption in clouds results in a non-negligible feedback to surface and mid-tropospheric temperatures globally (Jacobson, 2006). This in-cloud absorption may constitute up to 10% or more of the total temperature feedback from black carbon. Thus, aerosol absorption in clouds may have a large effect on the radiative balance of the atmosphere in the Amazon region.

ACPD
10, 24919–24960, 2010

3.2 Effect of land-atmosphere interactions

Biomass burning in the Amazon influences clouds in two ways – through smoke effects and through land use changes. Smoke particles can change cloud microphysics and heat the atmospheric cloud environment by absorbing sunlight, as described above. Land use changes that convert forest to pasture and cropland change surface heat and water vapor fluxes, which in turn affect cloud development. By dividing our data set into forested and deforested (pasture) subsets, we can begin to understand the relative effects of aerosols and land use changes on cloud properties, and especially how land use changes modify aerosol effects.

Table 1 shows average values of cloud, aerosol, and atmospheric profile parameters retrieved from the Level 2 MODIS products for both forest and pasture. Warm cloud fraction is higher for the pasture compared to the forest, which agrees with previous studies (Cutrim et al., 1995; Negri et al., 2004; Wang et al., 2009). In addition, a greater average cloud top pressure is observed for the pasture, which suggests more shallow cloud development over the pasture compared to the forest. This result also agrees with previous studies (Wang et al., 2000; Durieux et al., 2003; Chagnon et al., 2004; Correia et al., 2007; Wang et al., 2009). A consequence of deeper warm clouds over the forest is larger average liquid water paths over the forest. CWV is also higher over the forest, presumably due to the reduction in evapotranspiration over the pasture compared to the forest (Nobre et al., 1991; Correia et al., 2007). A lower value of atmospheric low-level stability is observed over the pasture, a parameter defined as the temperature at 850 hPa minus the temperature at 1000 hPa. The shorter roughness length and lower specific heat of the pasture result in greater surface heating, as supported by the higher 1000 hPa temperature compared to the forest. This heating is hypothesized to help spawn shallow cumulus clouds (Negri et al., 2004). The increase in surface temperature, and thus decrease in low-level atmospheric stability over deforested regions compared to forested regions in Table 1 agrees with other studies (Polcher and Laval, 1994; Correia et al., 2007). Average AOD is similar between the

ACPD
10, 24919–24960, 2010

two land cover types, a finding which is anticipated since aerosol concentrations are often spatially homogeneous, particularly at some distance away from concentrated smoke plumes. Frequency distributions of the variables in Table 1 for both forest and pasture are located in Supplement S.2.

Comparison of aerosol effects on CWV and clouds between different land cover types requires careful consideration of consistent sampling procedures. To perform this analysis, the same number of samples must be retrieved between forest and pasture for a given day for each AOD bin to ensure that weighting of the data by time of the year is consistent between both land cover types. The sampling process is as follows: First, for each parameter and each AOD bin, the number of samples for each day is determined for forest and pasture. For the land cover type (forested or pasture) with the minimum number of samples, the same number of samples is taken from the other land cover type. Because bin edges must be assigned beforehand using this procedure, the number of samples in each AOD bin is not consistent among all bins. The eight bins for both forest and pasture are equally spaced between 0.05 and 0.8.

Several randomized mixed forest and pasture subsamples are also conducted to assess the significance of the segregated land cover analysis. In each random subsample, the retrievals are randomly sampled between forest and pasture according to the relative proportion of forest and pasture retrievals in the actual data. This method results in no systematic segregation by land cover in each randomized subsample. Again, the data are processed such that the same number of samples is retained between forest and pasture for a given day for each AOD bin. Figure 8a illustrates the difference in the average sampled day of the year between pasture and forest in each AOD bin for both the actual data and the randomized subsamples. The difference is zero for all bins, indicating that the sampling procedure by definition does not weight the result by day of the year, thus there is no difference in the large-scale meteorology between the pasture and forest for each AOD bin.

One of the primary underlying assumptions in this study is that aerosols do not impact CWV through changes in evaporation and transpiration, but instead that CWV is

ACPD
10, 24919–24960, 2010

an indicator of the synoptic-scale meteorology. Aerosols could, in theory, affect evapotranspiration rates by changing both the magnitude and diffuse fractionation of radiation reaching the surface (Roderick et al., 2001; Jacobson, 2002; Yu et al., 2002; Knohl et al., 2008). Because deforested land has a leaf area index several times lower than forested land in addition to a significantly lower heat capacity, aerosols could affect the evapotranspiration and evaporation from the ground differently between forested and deforested land. We test this assumption by analyzing aerosol-CWV relationships separately over the forested area and deforested area. Table 1 indicates that the forest CWV is 0.2 cm higher on average than the pasture during our study period, which we assume is the result of differences in evapotranspiration. If we observe this difference correlated with aerosol, then we know that aerosol is modifying the CWV and our assumption of using CWV as a tracer for the large-scale meteorology in the former portion of the paper may be incorrect.

Figure 8b shows CWV binned by AOD over the pasture minus CWV binned by AOD over the forest for retrievals with non-zero cloud fractions. Error bars represent the square root of the sum of the pasture and forest standard errors squared. There is a lack of a significant trend in CWV differences with AOD. Instead, CWV is slightly higher over the forest compared to the deforested land for all AOD bins, an offset owed to the difference in evapotranspiration between pasture and forest. The random subsamples show no such offset since forest and pasture retrievals are randomly mixed. Figure 8b illustrates that the addition of aerosols below an AOD of 0.8 most likely does not influence evapotranspiration sufficiently to affect CWV differently between pasture and forest. The little variation that does exist between AOD bins is well within the standard error. More generally, the addition of aerosol below an AOD of 0.8 does not have a noticeable impact on CWV. Thus, changes in CWV may be attributed completely to changes in synoptic-scale conditions and seasonal cycles.

Figure 8c shows cloud fraction binned by AOD over the pasture minus cloud fraction binned by AOD over the forest. Absolute values of aerosol-cloud correlations over pasture and forest are not computed as they will be influenced by variations in CWV, similar

ACPD
10, 24919–24960, 2010

to Fig. 4. However, because the same number of retrievals is retained over the pasture and forest for each day in each AOD bin, computing cloud fraction differences between pasture and forest in each AOD bin will remove influences of the larger-scale meteorology. The cloud fraction difference between pasture and forest is always positive in Fig. 8c, indicating that cloud fraction is greater over the pasture than the forest, as also shown in Table 1. The figure also illustrates that there are increasingly more clouds over the pasture with increasing AOD, up to an AOD of 0.5. At this AOD threshold, the trend begins to flatten out, and even reverses slightly. The five random subsamples do not show higher average cloud fractions over the pasture compared to the forest, nor do they show a stronger microphysical aerosol forcing over the pasture, strengthening the significance of these results. What causes this noticeable dissimilarity in the aerosol effect between pasture and forest at AODs below 0.5? Because differences in CWV are likely not a driving factor due to the results of Fig. 8b, it is suggested that differences in low-level atmospheric stability may be at the root of the dissimilarity.

Figure 8d again shows the difference in cloud fraction binned by AOD between the pasture and forest similar to Fig. 8c, but also shows cloud fraction difference stratified by low-level stability derived from MODIS temperature products. The first case (red line) includes all retrievals where the low-level stability is less than −16 K over the pasture and greater than −16 K over the forest and the second case (blue line) includes all retrievals where the low-level stability is greater than −16 K over the pasture and less than −16 K over the forest. A threshold stability value of −16 K is selected because it is very close to the median stability over both pasture and forest. In addition, a temperature difference of 16 K or greater between 850 and 1000 hPa conservatively corresponds to an absolutely unstable atmosphere, according to a tropical standard atmosphere.

The red line represents the difference in cloud fraction between pasture and forest only for retrievals where the pasture is considered unstable and the forest is considered relatively more stable. In this case, the difference in cloud fraction between pasture and forest responds similarly to increasing AOD as the plot that includes all stabilities (black

ACPD
10, 24919–24960, 2010

line). This similarity is expected since the pasture is often more unstable than the forest (Supplement S.2). The blue line represents the reverse situation, retrievals where the forest is considered unstable and the pasture relatively more stable. Because this scenario is less likely, larger standard errors are observed. Unlike the first case that shows increasingly higher cloud fractions over the pasture compared to the forest with increasing AOD, this second case does not exhibit such a trend. The absence of an increasing trend may be attributed to the higher stability over the pasture compared to the forest – the microphysical forcing of clouds may be weaker in atmospheres that lack sufficient low-level instability. These results are consistent with findings in Yu et al. (2007).

Low-level stability appears to be a factor or a tracer for how aerosol modifies cloud fraction differently over forested and deforested surfaces. The greater instability that generally occurs over deforested land appears to encourage increases in cloud fraction with AOD. The statistical approach used here is limited, and cannot characterize the full mesoscale circulations thought to be responsible for the general differences in cloud fraction between forested and deforested surfaces (Wang et al., 2009). A proper 3-D cloud resolving model with adequate similations of surface fluxes and mesoscale circulations will be needed to explain the associations identified in Fig. 8d.

4 Conclusions

In this study, a 5° NE×5° WE region over Rondônia, Brazil was analyzed using high resolution aerosol, cloud, water vapor, and atmospheric temperature profile data from the Moderate Resolution Imaging Spectroradiometer (MODIS). Four years of data (2004–2007) during the biomass burning transition season (August–October) were compiled to analyze the effect of aerosols on warm cloud development. Several years of data were employed to gather a large enough dataset for analysis, and to smooth out inter-annual variability. MODIS observations illustrate that column water vapor (CWV) generally increased throughout the biomass burning season, while aerosol optical depth

ACPD
10, 24919–24960, 2010

(AOD) peaked during the middle of the season. These within-season trends in CWV and AOD may produce false correlations in cloud parameter versus AOD plots when all data throughout the biomass burning season are accumulated and analyzed together. By dividing the total period into subperiods, we found evidence that both large-scale meteorological factors traced by CWV and aerosol loading contributed to modification of the cloud fraction in our area of interest. To better account for this meteorological variability, data were stratified by CWV. When background CWV variability was removed, cloud fraction either increased or remained constant with AOD, depending on the CWV stratification. The largest increase in cloud fraction with AOD occurred at the highest value of CWV.

Decrease of cloud fraction with AOD, attributed to aerosol absorption effects, was not observed in the cloud fraction versus AOD plots once the data were stratified by CWV. However, the decrease was observed in the data divided into seasonal subsets, and associations between cloud fraction and aerosol were consistent with expectations that follow from the aerosol-cloud fraction feedback hypothesized by Koren et al. (2008). At lower cloud fractions when the aerosol has greater exposure to sunlight, the decrease of cloud fraction which we attributed to aerosol absorption effects increased in magnitude and was shifted to lower values of AOD.

Relationships between cloud optical depth (COD) and aerosol loading are more difficult to interpret. Plots of COD against AOD showed an initial increase of cloud optical depth, and then a turning point where clouds appeared to become optically thinner as aerosol loading increased. Increasing COD with aerosol may be attributed physically to the processes described by Twomey (1977), but the decrease of COD with AOD is best described by a combination of physical processes and satellite retrieval artifacts. Absorbing aerosol may cause cloud droplets to evaporate and clouds to thin. This is a legitimate physical process. On the other hand, the dark aerosol in and above the cloud may also decrease the cloud reflectance observed by the satellite, which the satellite retrieval interprets as a decrease in COD. As the cloud thins, subpixel holes in the cloud open, allowing darker reflectance from the surface beneath to again darken the cloud

ACPD
10, 24919–24960, 2010

reflectance measured by the satellite. Again the cloud reflectance is artificially too low, resulting in COD retrievals that are too low, which contributes to the strong decrease of COD with AOD observed in the data analysis. Assuming that the decreasing trend in COD with AOD is due to both radiative effects as well as retrieval artifacts, our results suggest that global climate models that do not include treatment of aerosol absorption in clouds are inaccurate over regions with high concentrations of absorbing aerosol.

This study also addressed the effect of aerosols on CWV and clouds over different land cover types. Land cover was segregated into forested and deforested surfaces using the MODIS land cover product, and the response of CWV to increasing AOD was analyzed between the forested and deforested land. We found that aerosols likely do not have a noticeable effect on CWV. Thus, it may be assumed that temporal changes in CWV are largely a function of the synoptic-scale meteorology and that aerosol is completely independent of CWV at the local level. The independence of CWV and AOD is an inherent assumption in the former portion of the paper, supported by the analysis in the latter portion of the paper.

This study showed that the relationship between cloud fraction and AOD is quite sensitive to land cover type. Microphysical effects appeared to be stronger over the deforested land compared to the forested land, increasing cloud fraction with AOD to a greater extent over the deforested land compared to the forest. The difference in the aerosol microphysical effect over the contrasting land cover types appears to be linked to the differing lower tropospheric stability over these two surfaces, but a full understanding of the complex interaction between aerosols, clouds, and land surface types cannot be achieved from the statistical approach used here. A 3-D cloud resolving model with adequate representation of surface-atmosphere exchange and ability to similate mesoscale circulations and cloud microphysical processes will be required.

The relationships shown here cannot, with certainty, be extrapolated to different times of the year or different regions of the world. These aerosol-cloud correlations are largely dependent on the physical and optical characteristics of the biomass burning aerosol (i.e. size distribution, composition); therefore, a different aerosol mixture

ACPD
10, 24919–24960, 2010

may or may not have a different impact on clouds. However, a similar analysis to this one over other biomass burning regions or heavily fossil-fuel polluted regions would be helpful in determining if these relationships could be extended more generally. More importantly, modeling-based studies are required to assign causation to the correlations found here.

Supplementary material related to this article is available online at: http://www.atmos-chem-phys-discuss.net/10/24919/2010/acpd-10-24919-2010-supplement.pdf.

Acknowledgement. This study was supported by NASA under Grant No. NN07AN25G and by the EPA under Agreement R833371, as well as by the NASA Earth Systems Science Fellowship and the Stanford Graduate Fellowship. We are grateful to James Coakley, Steven Platnick, and Rich Kleidman for helpful comments. We also thank Brent Holben and his staff for establishing and maintaining the two AERONET sites used in this investigation, Abracos Hill and Ji Paraná SE.

References

Ackerman, S. A., Strabala, K. I., Menzel, W. P., Frey, R. A., Moeller, C. C., and Gumley, L. E.: Discriminating clear sky from clouds with MODIS, J. Geophys. Res., 103(D24), 32141–32157, doi:10.1029/1998JD200032, 1998.

Ackerman, A. S., Toon, O. B., Stevens, D. E., Heymsfield, A. J., Ramanathan, V., and Welton, E. J.: Reduction of tropical cloudiness by soot, Science, 288, 1042–1047, 2000.

Albrecht, B. A.: Aerosols, cloud microphysics, and fractional cloudiness, Science, 245, 1227–1230, 1989.

Andreae, M. O., Artaxo, P., Brandão, C., et al.: Biogeochemical cycling of carbon, water, energy, trace gases, and aerosols in Amazonia: The LBA-EUSTACH experiments, J. Geophys. Res., 107(D20), 8066, doi:10.1029/2001JD000524, 2002.

Andreae, M. O., Rosenfeld, D., Artaxo, P., Costa, A. A., Frank, G. P., Longo, K. M., and Silva-Dias, M. A. F.: Smoking rain clouds over the Amazon, Science, 303, 1337–1342, 2004.

ACPD
10, 24919–24960, 2010

Brennan, J. I., Kaufman, Y. J., Koren, I., and Li, R.-R: Aerosol-cloud interaction – misclassification of MODIS clouds in heavy aerosol, IEEE T. Geosci. Remote, 43(4), 911–915, 2005.
Chagnon, F. J. F., Bras, R. L., and Wang, J.: Climatic shift in patterns of shallow clouds over the Amazon, Geophys. Res. Lett., 31, L24212, doi:10.1029/2004GL021188, 2004.
Correia, F. W. S., Alvalá, R. C. S., and Manzi, A. O.: Modeling the impacts of land cover change in Amazonia: a regional climate model (RCM) simulation study, Theor. Appl. Climatol., 93, 225–244, 2007.
Crutzen, P. J. and Andreae, M. O.: Biomass burning in the tropics: impact on atmospheric chemistry and biogeochemical cycles, Science, 250, 1669–1678, 1990.
Cutrim, E., Martin, D. W., and Rabin, R.: Enhancement of cumulus clouds over deforested lands in Amazonia, B. Am. Meteorol. Soc., 76, 1801–1805, 1995.
D'Almeida, C., Vorosmarty, C. J., Hurtt, G. C., Marengo, J. A., Dingman, S. L., and Keim, B. D.: The effects of deforestation on the hydrological cycle in Amazonia: a review on scale and resolution, Int. J. Climatol., 27, 633–647, 2007.
Davidi, A., Koren, I., and Remer, L.: Direct measurements of the effect of biomass burning over the Amazon on the atmospheric temperature profile, Atmos. Chem. Phys., 9, 8211–8221, doi:10.5194/acp-9-8211-2009, 2009.
Diner, D. J., Beckert, J. C., Reilly, T. H., et al.: Multi-angle Imaging SpectroRadiometer (MISR) instrument description and experiment overview, IEEE T. Geosci. Remote, 36(4), 1072–1087, 1998.
Dubovik, O., Holben, B. N., Eck. T. F., Smirnov, A., Kaufman, Y. J., King, M. D., Tanré, D., and Slutsker, I.: Variability of absorption and optical properties of key aerosol types observed in worldwide locations, J. Atmos. Sci., 59, 590–608, 2002.
Durieux, L., Machado, L. A. T., and Laurent, H.: The impact of deforestation on cloud cover over the Amazon arc of deforestation, Remote Sens. Environ., 86, 132–140, 2003.
Feingold, G., Jiang, H., and Harrington, J. Y.: On smoke suppression of clouds in Amazonia, Geophys. Res. Lett., 32, L02840, doi:10.1029/2004GL021369, 2005.
Feingold, G., Remer, L. A., Ramaprasad, J., and Kaufman, Y. J.: Analysis of smoke impacts on clouds in Brazilian biomass burning regions: an extension of Twomey's approach, J. Geophys. Res., 106(D19), 22907–22922, doi:10.1029/2001JD000732, 2001.
Friedl, M. A., Sulla-Menashe, D., Tan, B., Schneider, A., Ramankutty, N., Sibley, A., and Huang., X.: MODIS Collection 5 global land cover: algorithm refinements and characterization of new datasets, Remote Sens. Environ., 114, 168–182, 2010.

ACPD
10, 24919–24960, 2010

Gao, B.-C. and Kaufman, Y. J.: Water vapor retrievals using Moderate Resolution Imaging Spectroradiometer (MODIS) near-infrared channels, J. Geophys. Res., 108(D13), 4389, doi:10.1029/2002JD003023, 2003.
Giglio, L.: Characterization of the tropical diurnal fire cycle using VIRS and MODIS observations, Remote Sens. Environ., 108, 407–421, 2007.
Gunn, R. and Phillips, B. B.: An experimental investigation of the effect of air pollution on the initiation of rain, J. Meteorol., 14, 272–280, 1957.
Henderson-Sellers, A. and Gornitz, V.: Possible climatic impacts of land cover transformations, with particular emphasis on tropical deforestation, Climatic Change, 6, 231–257, 1984.
Holben, B. N., Eck, T. F., Slutsker, I., et al.: AERONET – a federated instrument network and data archive for aerosol characterization, Remote Sens. Environ., 66, 1–16, 1998.
Jacobson, M. Z.: Control of fossil-fuel particulate black carbon and organic matter, possibly the most effective method of slowing global warming, J. Geophys. Res., 107(D19), 4410, doi:10.1029/2001JD001376, 2002.
Jacobson, M. Z.: Effects of externally-through-internally-mixed soot inclusions within clouds and precipitation on global climate, J. Phys. Chem. A, 110(21), 6860–6873, 2006.
Kalnay, E., Kanamitsu, M., Kistler, R., et al.: The NCEP/NCAR 40-year reanalysis project, B. Am. Meteorol. Soc., 77, 437–471, 1996.
Kaufman, Y. J. and Fraser, R. S.: The effect of smoke particles on clouds and climate forcing, Science, 277, 1636–1639, 1997.
Kaufman, Y. J. and Koren, I.: Smoke and pollution aerosol effect on cloud cover, Science, 313, 655–658, 2006.
Kaufman, Y. J., Koren, I., Remer, L. A., Rosenfeld, D., and Rudich, Y.: The effect of smoke, dust, and pollution aerosol on shallow cloud development over the Atlantic Ocean, P. Natl. Acad. Sci. USA, 102(32), 11207–11212, 2005a.
Kaufman, Y. J. and Nakajima, T.: Effect of Amazon smoke on cloud microphysics and albedo – Analysis from satellite imagery, J. Appl. Meteorol., 32, 729–744, 1993.
Kaufman, Y. J., Remer, L. A., Tanré, D., Li, R.-R., Kleidman, R., Matoo, S., Levy, R., Eck, T. M., Holben, B. N., Ichoku, C., Martins, J. V., and Koren, I.: A critical examination of the residual cloud contamination and diurnal sampling effects on MODIS estimates of aerosol over ocean, IEEE T. Geosci. Remote, 43(12), 2886–2897, 2005b.
Kaufman, Y. J., Tanré, D., and Boucher, O.: A satellite view of aerosols in the climate system, Nature, 419, 215–223, 2002.

ACPD
10, 24919–24960, 2010

Kaufman, Y. J., Tanré, D., Remer, L. A., Vermote, E. F., Chu, A., and Holben, B. N.: Operational remote sensing of tropospheric aerosol over land from EOS moderate resolution imaging spectroradiometer, J. Geophys. Res., 102(D14), 17051–17067, doi:10.1029/96JD03988, 1997.

Khain, A., Rosenfeld, D., and Pokrovsky, A.: Aerosol impact on the dynamics and microphysics of deep convective clouds, Q. J. R. Meteorol. Soc., 131, 2639–2663, 2005.

King, M. D., Menzel, W. P., Kaufman, Y. J., Tanré, D., Gao, B.-C., Platnick, S., Ackerman, S. A., Remer, L. A., Pincus, R., and Hubanks, P. A.: Cloud and aerosol properties, precipitable water, and profiles of temperature and humidity from MODIS, IEEE T. Geosci. Remote, 41(2), 442–458, 2003.

Knohl, A. and Baldocchi, D. D.: Effects of diffuse radiation on canopy gas exchange processes in a forest ecosystem, J. Geophys. Res., 113, G02023, doi:10.1029/2007JG000663, 2008.

Koren, I., Feingold, G., and Remer, L. A.: The invigoration of deep convective clouds over the Atlantic: aerosol effect, meteorology or retrieval artifact?, Atmos. Chem. Phys., 10, 8855–8872, doi:10.5194/acp-10-8855-2010, 2010.

Koren, I., Kaufman, Y. J., Remer, L. A., and Martins, J. V.: Measurement of the effect of Amazon smoke on inhibition of cloud formation, Science, 303, 1342–1345, 2004.

Koren, I., Kaufman, Y. J., Rosenfeld, D., Remer, L. A., and Rudich, Y.: Aerosol invigoration and restructuring of Atlantic convective clouds, Geophys. Res. Lett., 32, L14828, doi:10.1029/2005GL023187, 2005.

Koren, I., Martins, J. V., Remer, L. A., and Afargan, H.: Smoke invigoration versus inhibition of clouds over the Amazon, Science, 321, 946–949, 2008.

Koren, I., Remer, L. A., and Longo, K.: Reversal of trend of biomass burning in the Amazon, Geophys. Res. Lett., 34, L20404, doi:10.1029/2007GL031530, 2007.

Levy, R. C., Remer, L. A., Mattoo, S., Vermote, E. F., and Kaufman, Y. J.: Second-generation operational algorithm: Retrieval of aerosol properties over land from inversion of moderate resolution imaging spectroradiometer spectral reflectance, J. Geophys. Res., 112, D13211, doi:10.1029/2006JD007811, 2007.

Lin, J. C., Matsui, T., Pielke Sr., R. A., and Kummerow, C.: Effects of biomass-burning-derived aerosols on precipitation and clouds in the Amazon Basin: a satellite-based empirical study, J. Geophys. Res., 111, D19204, doi:10.1029/2005JD006884, 2006.

Martins, J. A., Silva Dias, M. A. F., and Gonçalves, F. L. T.: Impact of biomass burning aerosols on precipitation in the Amazon: a modeling case study, J. Geophys. Res., 114, D02207,

ACPD
10, 24919–24960, 2010

doi:10.1029/2007JD009587, 2009.
Meskhidze, N., Remer, L. A., Platnick, S., Negrón Juárez, R., Lichtenberger, A. M., and Aiyyer, A. R.: Exploring the differences in cloud properties observed by the Terra and Aqua MODIS Sensors, Atmos. Chem. Phys., 9, 3461–3475, doi:10.5194/acp-9-3461-2009, 2009.
Myhre, G., Stordal, F., Johnsrud, M., Kaufman, Y. J., Rosenfeld, D., Storelvmo, T., Kristjansson, J. E., Berntsen, T. K., Myhre, A., and Isaksen, I. S. A.: Aerosol-cloud interaction inferred from MODIS satellite data and global aerosol models, Atmos. Chem. Phys., 7, 3081–3101, doi:10.5194/acp-7-3081-2007, 2007.
Nakajima, T. and King, M. D.: Determination of the optical thickness and effective particle radius of clouds from reflected solar radiation measurements. Part I: theory, J. Atmos. Sci., 47, 1878–1893, 1990.
Negri, A. J., Adler, R. F., Xu, L., and Surratt, J.: The impact of Amazonian deforestation on dry season rainfall, J. Climate, 17, 1306–1319, 2004.
Nobre, C. A., Mattos, L. F., Dereczynski, C. P., Tarasova, T. A., and Trosnikov, I. V.: Overview of atmospheric conditions during the Smoke, Clouds, and Radiation-Brazil (SCAR-B) field experiment, J. Geophys. Res., 103(D24), 31809–31820, doi:10.1029/98JD00992, 1998.
Nobre, C. A., Sellers, P. J., and Shukla, J.: Amazonian deforestation and regional climate change, J. Climate, 4, 957–988, 1991.
Platnick, S., King, M. D., Ackerman, S. A., Menzel, W. P., Baum, B. A., and Riedi, J. C.: The MODIS cloud products: algorithms and examples from Terra, IEEE T. Geosci. Remote, 41(2), 459–473, 2003.
Polcher, J. and Laval, K.: The impact of African and Amazonian deforestation on tropical climate, J. Hydrology (Amsterdam), 155, 389–405, 1994.
Ramanathan, V., Chung, C., Kim, D., Bettge, T., Buja, L., Kiehl, J. T., Washington, W. M., Fu, Q., Sikka, D. R., and Wild, M.: Atmospheric brown clouds: impacts on South Asian climate and hydrological cycle, P. Natl. Acad. Sci. USA, 102(15), 5326–5333, 2005.
Remer, L. A., Kaufman, Y. J., Holben, B. N., Thompson, A. M., and McNamara, D.: Biomass burning aerosol size distribution and modeled optical properties, J. Geophys. Res., 103(D24), 31879–31891, doi:10.1029/98JD00271, 1998.
Remer, L. A., Kaufman, Y. J., Tanré, D., Matoo, S., Chu, D. A., Martins, J. V., Li, R.-R., Ichoku, C., Levy, R. C., Kleidman, R. G., Eck, T. F., Vermote, E., and Holben, B. N.: The MODIS aerosol algorithm, products and validation, J. Atmos. Sci., 62, 947–973, 2005.
Roderick, M. L., Farquhar, G. D., Berry, S. L., and Noble, I. R.: On the direct effect of clouds

ACPD
10, 24919–24960, 2010

and atmospheric particles on the productivity and structure of vegetation, Oecologia, 129, 21–30, 2001.
Rosenfeld, D., Lohmann, U., Raga, G. B., O'Dowd, C. D., Kulmala, M., Fuzzi, S., Reissell, A., and Andreae, M. O.: Flood or drought: how do aerosols affect precipitation?, Science, 321, 1309–1313, 2008.
Roy, S. B. and Avissar, R.: Impact of land use/land cover change on regional hydrometeorology in Amazonia, J. Geophys. Res., 107(D20), 8037, doi:10.1029/2000JD000266, 2002.
Salomonson, V. V., Barnes, W. L., Maymon, P. W., Montgomery, H. E., and Ostrow, H.: MODIS – advanced facility instrument for studies of the Earth as a system, IEEE T. Geosci. Remote, 27(2), 145–153, 1989.
Seemann, S., Li, J., Menzel, P., and Gumley, L. E.: Operational retrieval of atmospheric temperature, moisture, and ozone from MODIS infrared radiances, J. Appl. Meteor., 42(8), 1072–1091, 2003.
Segal, M., Avissar, R., McCumber, M. C., and Pielke, R. A.: Evaluation of vegetation effects on the generation and modification of mesoscale circulations, J. Atmos. Sci., 45, 2268–2293, 1988.
Squires, P.: The microstructure and colloidal stability of warm clouds, Part I. The relation between structure and stability, Tellus, 10, 256–271, 1958.
Twomey, S.: The influence of pollution on the shortwave albedo of clouds, J. Atmos. Sci., 34, 1149–1152, 1977.
Wang, J., Bras, R. L., and Eltahir, E. A. B.: The impact of observed deforestation on the mesoscale distribution of rainfall and clouds in Amazonia, J. Hydrometeorol., 1, 267–286, 2000.
Wang, J., Chagnon, F. J. F, Williams, E. R., Betts, A. K., Renno, N. O., Machado, L. A. T., Bisht, G., Knox, R., and Bras, R. L.: Impact of deforestation in the Amazon basin on cloud climatology, P. Natl. Acad. Sci. USA, 106(10), 2670–2674, 2009.
Wen, G., Marshak, A., and Cahalan, R. F.: Impact of 3-D clouds on clear sky reflectance and aerosol retrieval in a biomass burning region of Brazil, IEEE Geosci. Remote S., 3(1), 169–172, 2006.
Wilcox, E. M., Harshvardhan, and Platnick, S.: Estimate of the impact of absorbing aerosol over cloud on the MODIS retrievals of cloud optical thickness and effective radius using two independent retrievals of liquid water path, J. Geophys. Res., 114, D05210, doi:10.1029/2008JD010589, 2009.

ACPD
10, 24919–24960, 2010

Williams, E., Rosenfeld, D., Madden, N., et al.: Contrasting convective regimes over the Amazon: implications for cloud electrification, J. Geophys. Res., 107(D20), 8082, doi:10.1029/2001JD000380, 2002.

Winker, D. M., Pelon, J. R., and McCormick, M. P.: The CALIPSO mission: spaceborne lidar for observation of aerosols and clouds, Proc. SPIE, 4893(1), doi:10.1117/12.466539, 2003.

Yu, H., Fu, R., Dickinson, R. E., Zhang, Y., Chen, M., and Wang, H.: Interannual variability of smoke and warm cloud relationships in the Amazon as inferred from MODIS retrievals, Remote Sens. Environ., 111, 435–449, 2007.

Yu, H., Liu, S. C., and Dickinson, R. E.: Radiative effects of aerosols on the evolution of the atmospheric boundary layer, J. Geophys. Res., 107(D12), 4142, doi:10.1029/2001JD000754, 2002.

Zhang, Y., Fu, R., Yu, H., Dickinson, R. E., Juarez, R. N., Chin, M., and Wang, H.: A regional climate model study of how biomass burning aerosol impacts land-atmosphere interactions over the Amazon, J. Geophys. Res., 113, D14S15, doi:10.1029/2007JD009449, 2008.

ACPD

10, 24919–24960, 2010

Table 1. Average warm cloud and atmospheric profile statistics for both forested and deforested land in our study region. The averaging period is for August through October for the years 2004 through 2007.

	Forested	Deforested
Cloud fraction (–)	0.52	0.63
Cloud optical depth (–)	8.95	8.07
Cloud top pressure (hPa)	796.4	817.9
Cloud effective radius (μm)	15.9	14.7
Cloud water path (g/m^2)	81.3	68.0
Column water vapor (cm)	3.76	3.54
850 hPa temperature (K)	292.6	293.0
1000 hPa temperature (K)	307.2	311.4
Low-level stability [temperature 850 hPa minus temperature 1000 hPa (K)]	−14.6	−18.4
AOD at 550 nm (–)	0.92	0.89

ACPD
10, 24919–24960, 2010

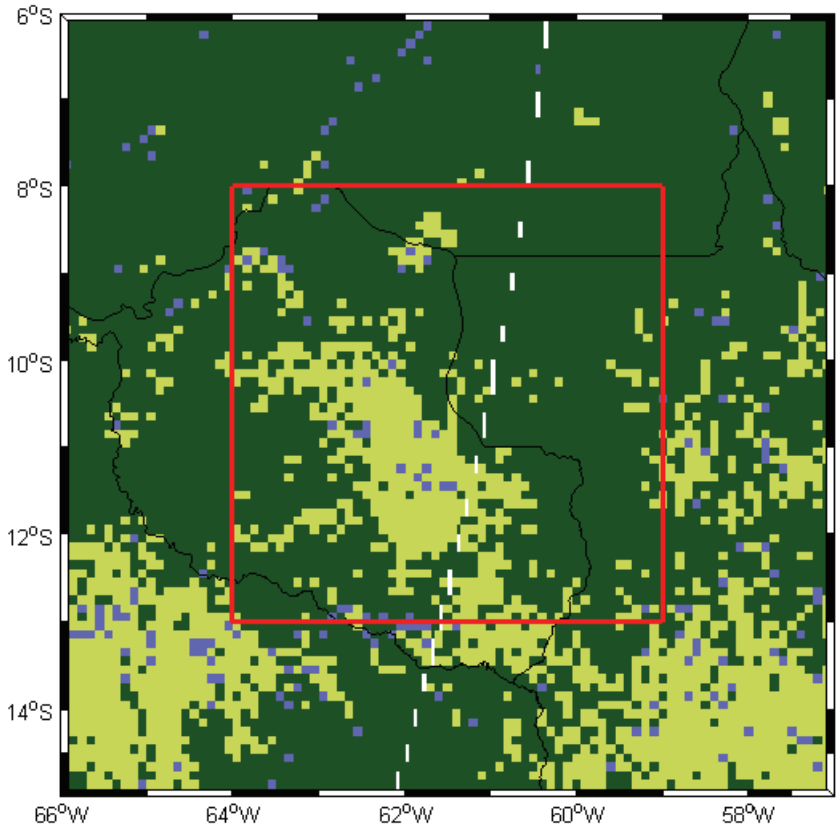

Fig. 1. Land cover classifications for the year 2004. Green pixels represent evergreen forests and yellow pixels represent deforested land (pasture). Blue pixels represent land classifications that are not included in either of these two categories. The 5°×5° study region is outlined with a red box. On average between 2004 and 2007, roughly 73% of our study region is classified as forest and 25% of our study region is classified as deforested land.

ACPD
10, 24919–24960, 2010

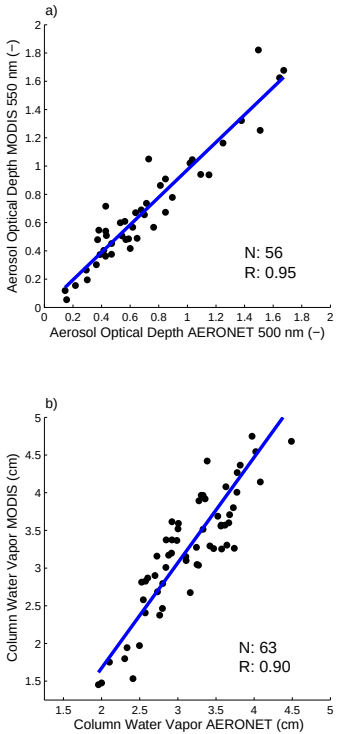

Fig. 2. **(a)** Comparison of co-located MODIS aerosol optical depth retrievals with automatic sun/sky radiometers of the Aerosol Robotic Network (AERONET) at Abracos Hill (62.358° W, 10.760° S) and Ji Paraná SE (61.852° W, 10.934° S) for days used in the study during the months of August through October, for the years 2004 through 2007. These two sites are within our 5°×5° study region. **(b)** Comparison of co-located Level 2 MODIS column water vapor retrievals with automatic AERONET retrievals for the same time period as in (a). The number of points (*N*) in each plot and correlation coefficients (*R*) between MODIS and AERONET data are also included.

ACPD
10, 24919–24960, 2010

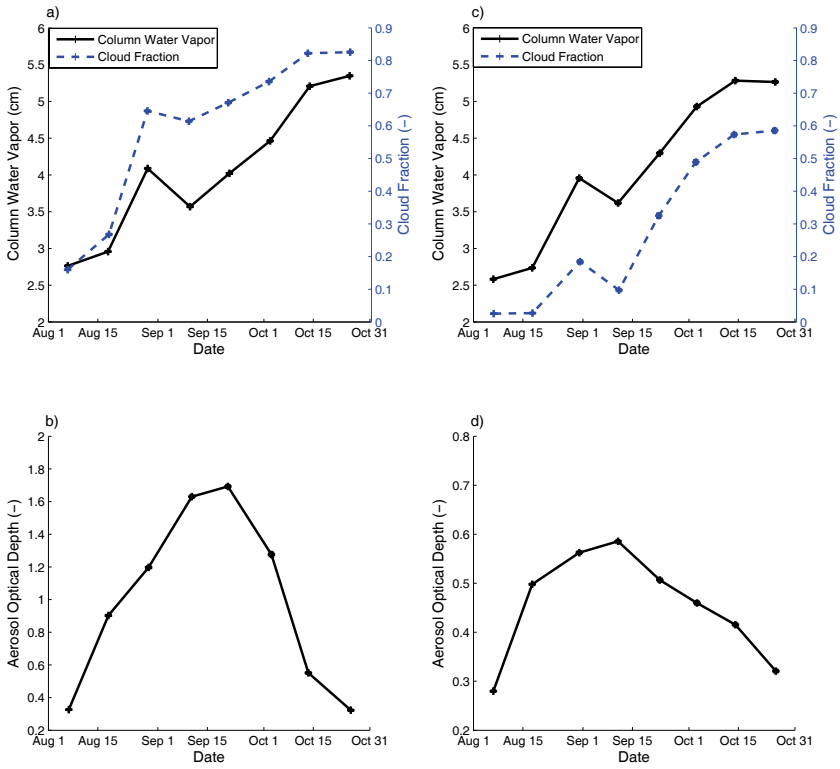

Fig. 3. **(a)** Column water vapor and warm cloud fraction binned by day of the year for the months of August through October, for the years 2004 through 2007. Data are accumulated into eight bins of equal width between 1 August and 31 October. **(b)** Aerosol optical depth at 550 nm binned by day of the year for the same time period as in (a). **(c)** Same as (a) but for AODs equal to or below 0.8. **(d)** Same as (b) but for AODs equal to or below 0.8. Error bars are included but are too narrow to be visible. The number of points (N) incorporated in each bin is provided in Supplement S.1.

ACPD
10, 24919–24960, 2010

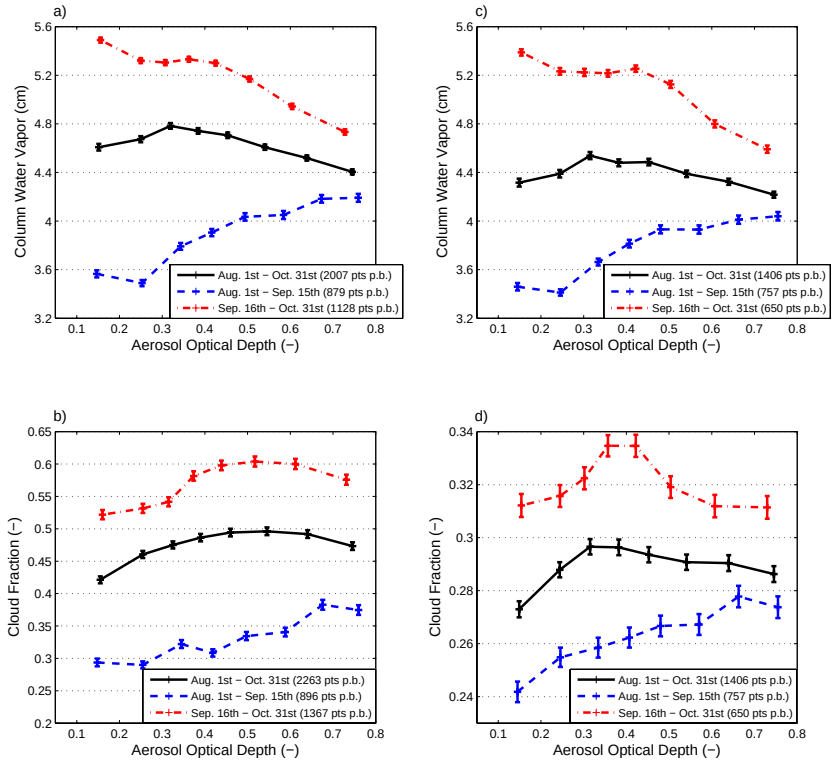

Fig. 4. **(a)** Column water vapor binned by aerosol optical depth for all co-located warm cloud retrievals for the months of August through October, for the years 2004 through 2007. Error bars denote the standard error in each bin. **(b)** Cloud fraction binned by aerosol optical depth for all warm cloud retrievals for the same time period as in (a). **(c)** Column water vapor binned by aerosol optical depth for all co-located warm cloud retrievals with cloud fractions less than 0.5. (d) Cloud fraction binned by aerosol optical depth for all warm cloud retrievals with cloud fractions less than 0.5. The number of points (N) included each bin is noted in the legend.

ACPD
10, 24919–24960, 2010

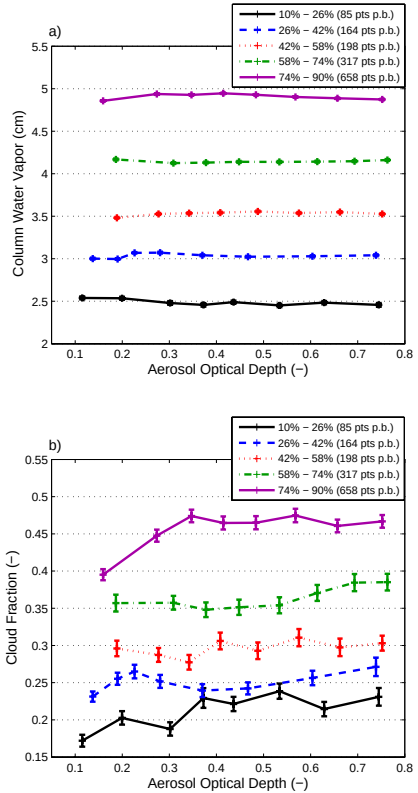

Fig. 5. **(a)** Column water vapor and **(b)** cloud fraction binned by aerosol optical depth for all co-located warm cloud retrievals for different percentile groupings of column water vapor. Data represent the months of August through October, for the years 2004 through 2007. The number of points (*N*) included each bin is noted in the legend.

ACPD
10, 24919–24960, 2010

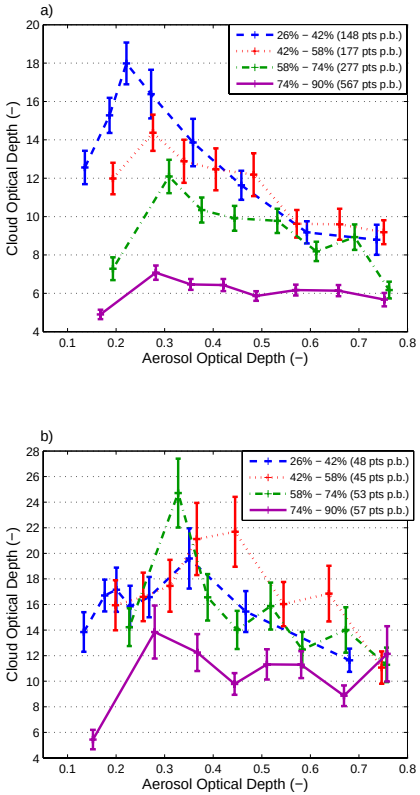

Fig. 6. **(a)** Liquid cloud optical depth binned by aerosol optical depth for different percentile groupings of column water vapor for the months of August through October, for the years 2004 through 2007. **(b)** Same as (a) but only for retrievals with cloud top pressures between 800 hPa and 850 hPa. The number of points (*N*) included each bin is noted in the legend.

ACPD
10, 24919–24960, 2010

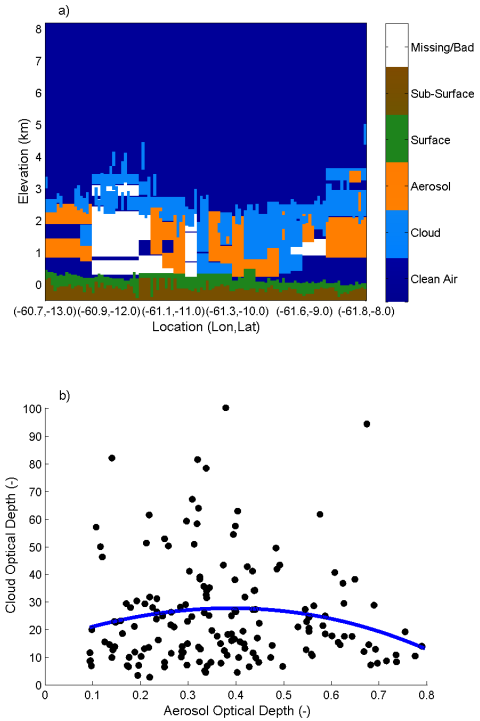

Fig. 7. (a) Vertical Feature Mask from the CALIPSO lidar on a path through the study region for a single day during the study period, 12 August 2006. On this day, clouds mostly form near the top of the aerosol layer. Clouds that extend throughout the column may be misclassified heavy aerosol plumes. **(b)** Scatter plot of MODIS Aqua cloud optical depth versus aerosol optical depth on the same day as in (a), throughout the 5°×5° study region for cloud top pressures between the 5th and 50th percentiles (784–846 mb). Low clouds likely embedded within the aerosol layer are removed (>50th percentile) in addition to high clouds which may be above the influence of aerosols (<5th percentile), leaving 165 retrievals for analysis. A least squares third-degree polynomial that best fits the data is also plotted.

ACPD
10, 24919–24960, 2010

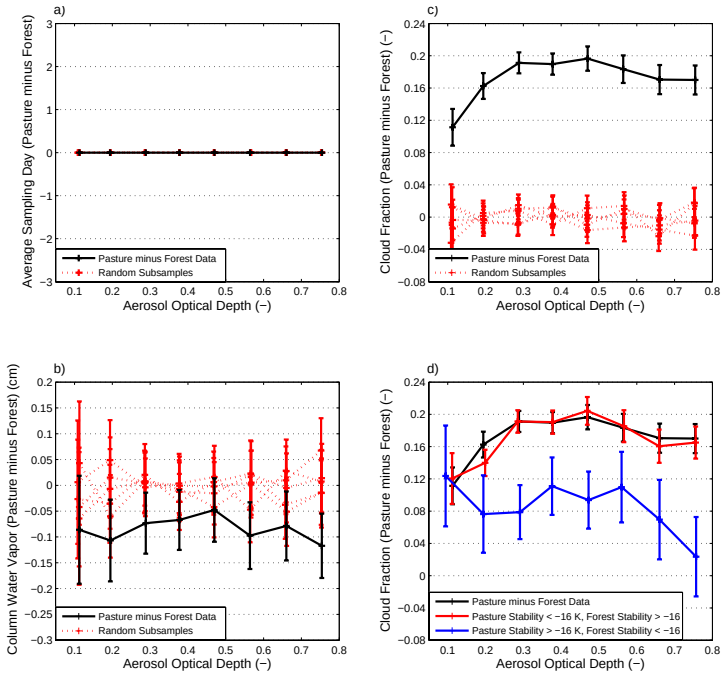

Fig. 8. **(a)** Difference between the average sampled day of the year in each AOD bin for the pasture and forest sites. In panels **(a–c)** red dotted lines represent the results of five random subsamples, where retrievals over forest and pasture are mixed. Data represent the months August through October, for the years 2004 through 2007. (b) Differenced column water vapor binned by AOD between pasture and forest land cover types. (c) Differenced cloud fraction binned by AOD between pasture and forest land cover types. **(d)** Black line: Same as **(c)**, red and blue lines: Differenced cloud fraction binned by AOD stratified by low-level stability, defined as the temperature at 850 hPa minus the temperature at 1000 hPa. The stratification values are different between pasture and forest for each stratification case. The number of points (N) incorporated in each bin is provided in Supplement S.3.

ACPD
10, 24919–24960, 2010